ACS Macro Letters

Letter

pubs.acs.org/macroletters

Universal Scaling of Polymer Diffusion in Nanocomposites

Jihoon Choi,[†] Michael J. A. Hore,[†,‡] Jeffrey S. Meth,[§] Nigel Clarke,[∥] Karen I. Winey,[†] and Russell J. Composto*,[†]

[†]Department of Materials Science and Engineering, University of Pennsylvania, Philadelphia, United States

[§]DuPont Nanocomposite Technologies, Central Research and Development, E.I. DuPont de Nemours and Co., Inc., P.O. Box 400, Wilmington, Delaware, United States

[∥]Department of Physics and Astronomy, University of Sheffield, Sheffield, S3 7RH, United Kingdom

Supporting Information

ABSTRACT: Nanoparticles are new and valuable additives that can favorably tune thermomechanical, electric, optical, and magnetic properties of polymeric materials. The addition of nanoparticles can also enhance or slow down polymer dynamics depending on the mixture thermodynamics and key length scales, namely, nanoparticle size, interparticle spacing (ID), and the polymer radius of gyration (R_g). Presently, a framework for understanding how nanoparticles affect polymer dynamics is not available, in part, because of a lack of wide-ranging experimental studies. Here, tracer diffusion is studied in model nanocomposites containing silica nanoparticles grafted with either polymer brushes (soft nanoparticles) or short ligands (hard nanoparticles). Over a wide range of tracer molecular weights and nanoparticle loadings, the normalized diffusion coefficient collapses onto a universal curve for both soft and hard nanoparticles when plotted against a confinement parameter, defined as ID/R_g, which accounts for tracer penetration into the brush. These experimental results provide new insights into the fundamental principles required to construct predictive models of polymer dynamics in nanocomposites.

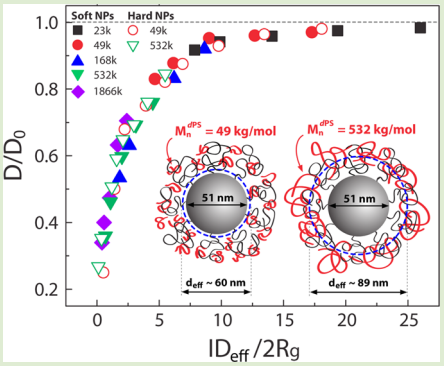

Nanoparticles (NPs) can enhance mechanical and thermal properties and impart host materials with novel properties attractive for biological, energy, and sensing applications, to name a few.[1−4] In particular, NPs have been widely used to modify and improve polymer properties by assembling them into nanoscale structures with a tunable length scale and morphology (i.e., dispersed or aggregated).[5,6] A main reason for the growing interest in polymer nanocomposites (PNCs) is the recent availability of functional NPs that impart materials with unique electric, optical, and magnetic properties.[7−9] Furthermore, with advances in chemistry, NPs are now available in a variety of shapes, sizes, and compositions.[10,11] Similarly, advances in surface modification of NPs provide a powerful approach for controlling NP/matrix interactions at the molecular size.[12−14] Namely, NP surfaces can be modified by long and flexible polymer brushes covalently anchored to the NP surface with controlled spacing (i.e., grafting density). Although they can enhance the dispersion of NPs in a polymer, the polymer brush itself can modify material properties. For example, the brush length can be used to fine-tune NP−NP spacing to control coupling of surface plasmon resonances and thereby optical adsorption in PNCs containing metallic NPs.[15]

How we process PNCs into bulk materials or films depends on the mobility of the molecules in the presence of NPs, which can be grafted with a short ligand (i.e., hard NP) or polymer brush (i.e., hard or soft NP). Although nanocomposites exhibit characteristic dynamics across a wide range of temperature and time scale as in neat polymers, a unified picture that describes polymer dynamics in the presence of NPs is not available. Experimental and theoretical studies have reported an immobilized polymer layer for systems having favorable interactions between polymer and NPs.[16,17] Other studies indicate that local segmental dynamics in the vicinity of NPs are unaffected.[18,19] Moreover, both experiments and simulations report a mobility gradient for chains adjacent to NPs.[20−22] However, when we turn our attention to the center-of-mass dynamics as measured by polymer diffusion at a longer time scale, the distinction between hard and soft NPs depends on the matrix polymer as well as the NPs. For example, it is no longer sufficient to designate a NP as hard or soft solely by the presence or absence of grafted polymer chains on the NP because "*soft*" requires that matrix chains penetrate into the polymer brush, which responds by stretching further into the matrix. Namely, at a fixed brush length, the NP can function as a hard or soft NP if the matrix length is relatively long or short, respectively. Thus, studies of center of mass diffusion in PNCs containing polymer brush grafted NPs can provide an understanding of the fundamental parameters that must be captured by predictive models of polymer dynamics.

Received: February 12, 2013
Accepted: May 14, 2013
Published: May 20, 2013

   dx.doi.org/10.1021/mz400064w | *ACS Macro Lett.* 2013, 2, 485−490

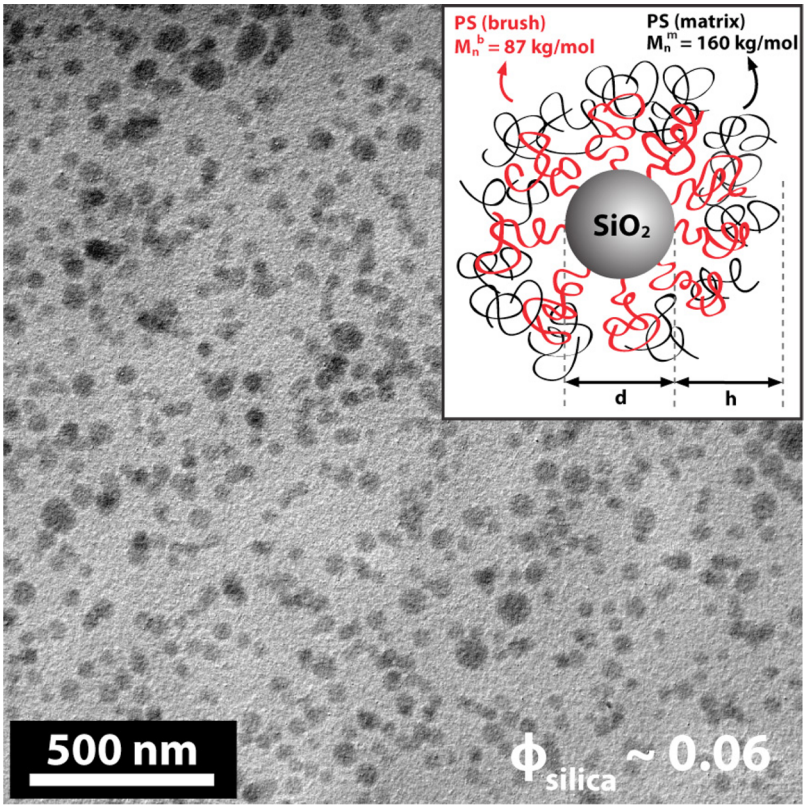

Figure 1. Morphology of SiO_2−PS87k:PS nanocomposites. Cross-sectional TEM micrograph depicting the distribution of silica cores (d = 51 nm) for a nanocomposite film with $\phi_{silica} \sim 0.06$. Inset shows the scheme of a polystyrene-grafted silica nanoparticle (M_n^b = 87 kg mol^{-1}, red) dispersed in a polystyrene matrix (M_n^m = 160 kg mol^{-1}, black).

By using this ability to transform NPs from hard to soft by reducing the matrix molecular weight, we have uncovered a universal scaling rule for polymer diffusion in nanocomposites. We previously found that PNCs with hard NPs ($d \sim$ 13 and 29 nm) capped with a phenyl group showed a monotonic slowing down of polymer dynamics with increasing confinement across a wide range of SiO_2 NP concentration (ϕ_{silica} = 0−0.5) and tracer molecular weight (M_n^t = 49−532 kg mol^{-1}).[23,24] In this paper, we investigate and compare diffusion in polymer nanocomposites containing hard and soft NPs and find that a simple confinement parameter can capture the correlation between dynamics and structure. Surprisingly, by defining an effective particle diameter that accounts for tracer penetration into the brush in soft NP systems, polymer diffusion is found to be universal for both hard and soft NPs over a wide NP concentration and tracer molecular weight. This universal scaling behavior highlights the importance of interparticle distance between hard/soft NPs relative to the size of the diffusing chain.

To determine tracer diffusion coefficients, the volume fraction profiles of deuterated polystyrenes (dPS) in PNCs are measured by elastic recoil detection (ERD).[25] Bilayer samples were prepared with a top dPS (M_n^t = 23−1866 kg mol^{-1}) layer of 15 nm on a thick polystyrene (PS; M_n^m = 160 kg mol^{-1}, PDI = 1.05) nanocomposite containing either hard or soft nanoparticles (ϕ_{silica} = 0−0.5). Bilayers were annealed in a vacuum oven at T = 170 °C for a few minutes to hours. Hard NPs were prepared by modifying SiO_2 NPs (51 nm diameter, 0.22 dispersity) with low molecular weight initiator (2-bromo-isobutylate derivative) and are denoted as SiO_2−I. Using the same SiO_2 NPs, soft NPs are functionalized with polystyrene brushes (M_n^b = 87 kg mol^{-1} and ρ = 0.52 chains/nm^2) grown by surface-initiated atom transfer radical polymerization (SI-ATRP) and denoted as SiO_2−PS87k.[26−28] The inset of Figure 1 depicts the brush-grafted (red) NP with diameter d and brush thickness h in a PS matrix (black). To understand how tracer diffusion depends on the unoccupied volume in the PNC, the interparticle distance (ID) was precisely controlled by tuning the volume fraction of SiO_2−PS87k or SiO_2−I, while maintaining a uniform dispersion of NPs. The cross-sectional transmission electron micrograph in Figure 1 shows that nanoparticles are well dispersed in a PS matrix at $\phi_{silica} \sim 0.06$. The surface modification of the NPs using polymer brushes and low molecular ligands facilitates the uniform dispersion in PS even up to extremely high loading, ϕ_{silica} = 0.5.

For the annealed bilayer (Figure 2a, inset), a representative dPS volume fraction profile is shown in Figure 2a, where the solid line represents the best fit to the experimental data (circles). Using Fick's second law and appropriate boundary and initial conditions, $\phi_{dPS}(x)$ is given by

$$\phi_{dPS}(x) = \frac{1}{2}\left[\mathrm{erf}\left(\frac{l-x}{\sqrt{4Dt}}\right) + \mathrm{erf}\left(\frac{l+x}{\sqrt{4Dt}}\right)\right] \quad (1)$$

where erf, t, and l are the error function, annealing time, and initial dPS thickness, respectively. Equation 1 is convoluted with the instrumental depth resolution and chi squared fitting is used to determine the best fit (solid line), which corresponds to $D = 1.8 \times 10^{-14}$ cm^2 s^{-1} in Figure 2a.[29,30] Figure 2b shows the tracer diffusion coefficients for five tracer molecular weights (M_n^t = 23−1866 kg mol^{-1}) as a function of the volume fraction of silica (ϕ_{silica} = 0 to ~0.06). At fixed ϕ_{silica}, the diffusion

dx.doi.org/10.1021/mz400064w | ACS Macro Lett. 2013, 2, 485−490

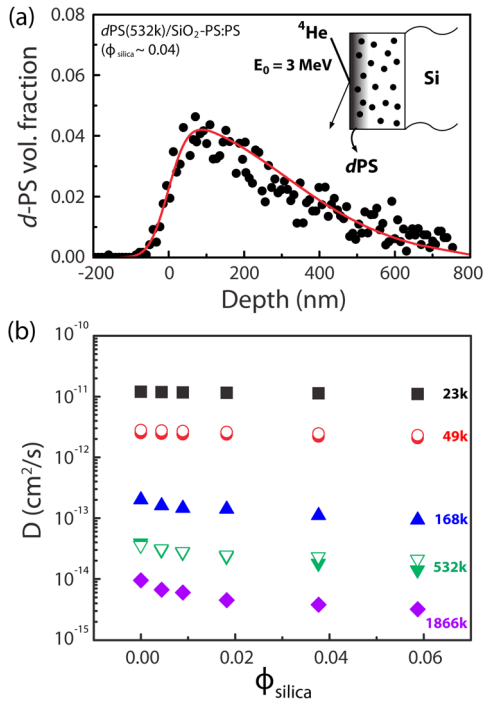

Figure 2. Tracer diffusion coefficients determined by the volume fraction profiles of dPS in SiO_2−PS87k:PS nanocomposites. (a) Depth profile of dPS(532k) in SiO_2−PS87k:PS ($\phi_{silica} \sim 0.04$) measured using ERD to investigate the effect of the polymer brushes on tracer diffusion at 170 °C. Solid line is a fit to the experimental profile that yields a diffusion coefficient of $D = 1.8 \times 10^{-14}$ cm^2 s^{-1}. Inset shows the ERD geometry with 3 MeV He^+ impinging on the bilayer and recoiling deuterium from dPS. (b) Diffusion coefficients for M_n^t = 23, 49, 168, 532, and 1866 kg mol^{-1} at 170 °C as a function of the volume fraction of silica. Closed and open symbols represent dPS diffusion in nanocomposites with soft (SiO_2−PS87k) and hard (SiO_2−I) nanoparticles, respectively. The uncertainty in D is less than the symbol size.

coefficient decreases as the molecular weight increases. For diffusion of entangled polymers in unfilled entangled melts ($\phi_{silica} = 0$), the reptation model describes the chain as moving along its own contour while lateral motions are constrained by entanglements which define a surrounding tube. The time to leave this tube defines the longest relaxation or reptation time.[31] For each dPS molecular weight, the diffusion coefficient decreases as ϕ_{silica} increases. In particular, a more pronounced decrease of the tracer diffusion coefficient was observed for high molecular weight dPS (168k, 532k, 1866k) compared to low molecular weight dPS (23k, 49k), indicating that larger molecules are more constrained by the immobile NPs. Thus, these experimental studies indicate that relevant parameters in modeling polymer dynamics should include the probe size (i.e., radius of gyration, R_g) and the confinement size imposed by the impenetrable objects. This constriction can be approximated by assuming a random distribution of NPs in 3D with an average interparticle spacing given by $ID = d[((2)/(\pi\varphi_{silica}))^{1/3}(\exp(\ln \sigma)^2) - 1]$, where d is the number average particle diameter and σ is the polydispersity of nanoparticles.[24] If a modified reptation model can be used to predict dynamics in PNCs, a fundamental question is whether the observed slowing down (Figure 2b) can be explained by a decrease in tube diameter due to the NPs. In recent studies, a reduction in tube diameter was observed, although a relatively high volume fraction, ∼0.20, of hard NPs (d = 17 nm) was required.[19]

Hard NPs have a well-defined interface with diffusing tracer molecules that can closely approach the hard NP surface, whereas soft NPs with polymer brushes display an interface that depends on the length of the tracer relative to the brush. Namely, shorter tracer chains can "wet" a long brush, whereas longer tracer chains are excluded. At equal loadings a difference between diffusion in PS matrices containing hard (open symbols) and soft (closed symbols) NPs is apparent upon comparing low and high tracer molecular weights in Figure 2b. Specifically, the tracer diffusion of dPS(49k) into hard nanoparticle nanocomposites ($\phi_{silica} \cong 0.06$) is very similar to the soft nanoparticle case, increasing by less than 10%. However, diffusion of the dPS(532k) D increases by ∼50% compared to the soft nanoparticles. Namely, the diffusion of dPS(532k) in a PS matrix containing soft NPs is slower than in the hard NP case, while the diffusion coefficients for dPS(49k) are statistically similar for hard and soft NPs. In the latter case, the short tracer can penetrate the brush and accordingly diffuses in a similar manner as the hard particle case. However, the long tracer is unable to penetrate the brush, revealing the presence of the impenetrable polymer brush layer at the particle−polymer interface. Thus, the penetration by the probe molecules should be taken into account to accurately determine the effective interparticle distance, $ID_{eff} = ID - 2h_{eff}$, where h_{eff} approximates the distance of closest approach for a tracer molecule in the brush.

To quantify the interfacial characteristics, self-consistent field theory (SCFT) was used to determine the monomer density profiles of the brush, matrix, and tracer chains near the NP surface.[32] Figure 3a,b shows the profiles as a function of distance, normalized by the unperturbed brush size, for a PS(87k) brush in contact with the PS(160k) matrix and either the dPS(23k) or dPS(532k) tracer chains at φ_t = 0.1. In general, the broad interface between brush (blue) and matrix (black) chains indicates that the wetting of the matrix into the brush is responsible for the excellent dispersion of SiO_2−PS87k in PS(160k) shown in Figure 1.[33−35] Furthermore, these profiles demonstrate the profound influence that the molecular weight of dPS has on the spatial distribution of the tracer molecules near the NP surface. Figure 3a shows that dPS(23k) penetrates deep into the brush at a nearly uniform concentration (∼10%), indicating that dPS(23k) diffusion in hard and soft NPs should be similar ($h_{eff} \sim 0$). In contrast, dPS(532k) is depleted around the NP surface, as shown in Figure 3b. This limited penetration is determined by a balance between the (i) conformational entropy penalty for long matrix chains within the brush and (ii) translational entropy gain of the tracer. Thus, for similar brush and tracer molecules, as tracer size increases, it penetrates less deeply into the polymer brush due to steric exclusion. Therefore, the dPS profiles determined by SCFT can be used to define an effective particle diameter, $d_{eff} = d + 2h_{eff}$, where h_{eff} is the brush thickness defined at φ_t = 0.05 (red arrow). Table 1 shows the values of d_{eff} for the five tracer molecular weights where the calculations were carried out in two dimensions. Note that the 3D SCFT calculation exhibits very similar results to the 2D calculations.

To verify the SCFT results (Figure 3a,b), small-angle neutron scattering (SANS) experiments were performed for the same dPS(23k) and dPS(532k) systems and the interfacial profiles are found to be in excellent agreement. Figure 3c shows the SANS spectra at $\phi_{silica} \sim 0.05$ for mixtures of PS(160k) and

dx.doi.org/10.1021/mz400064w | ACS Macro Lett. 2013, 2, 485−490

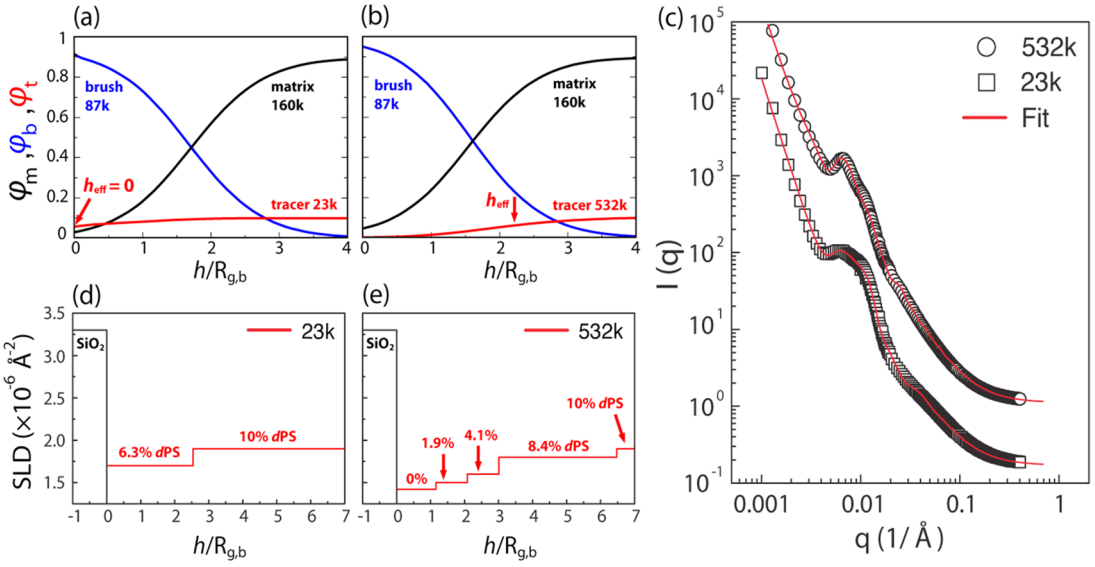

Figure 3. Penetration of short dPS(23k) and long dPS(532k) tracer molecules into the PS brush on the NPs. (a, b) Self-consistent field theory calculations showing the volume fraction profiles of dPS(23k) and dPS(532k), respectively, as a function of the distance from the silica particle surface normalized by the brush radius of gyration ($R_{g,b}$). The effective brush thickness h_{eff}, defined at $\varphi_t = 0.05$, represents how deeply the tracer can penetrate the brush. The dPS(23k) penetrates the brush fully ($h_{eff} \sim 0$) and therefore diffusion in SiO_2−PS87k and SiO_2−I systems are expected to be similar. However, the dPS(532k) is excluded from the inner brush resulting in a reduction of the interparticle spacing in the SiO_2−PS87k:PS system relative to the hard NP case. (c) SANS spectra for the SiO_2−PS87k:PS nanocomposites ($\phi_{silica} = 0.05$) blended with 10 vol % of dPS (M_n^t = 23 kg mol^{-1}, square) and dPS (M_n^t = 532 kg mol^{-1}, circle). The lines represent a core−shell fit corresponding to (d) single shell and (e) four shell models for dPS(23k) and dPS(532k), respectively. (d, e) Scattering length density (ξ) profiles for the particle−brush system with a single shell ($\xi_{6.3\%\ dPS} = 1.7 \times 10^{-6}$ Å^{-2}) and four shells ($\xi_{0\%\ dPS} = 1.42 \times 10^{-6}$ Å^{-2}, $\xi_{1.9\%\ dPS} = 1.5 \times 10^{-6}$ Å^{-2}, $\xi_{4.1\%\ dPS} = 1.6 \times 10^{-6}$ Å^{-2}, $\xi_{8.4\%\ dPS} = 1.8 \times 10^{-6}$ Å^{-2}) surrounding the NP. The polymer matrix corresponds to $\xi_{10\%\ dPS} = 1.9 \times 10^{-6}$ Å^{-2}.

Table 1. For the Five Tracer Molecular Weights (M_n^t), SCFT Calculations of the Effective Brush Thickness, h_{eff}, Relative to the Unperturbed Brush Length, $R_{g,b}$, and the Effective Particle Size d_{eff} (= $d + 2h_{eff}$)[a]

	M_n^t (g mol^{-1})	M_n^t/M_n^b	$h_{eff}/R_{g,b}$	d_{eff} (nm)
23k	23000	0.22	0.0	51.0
49k	49000	0.47	0.5	59.4
168k	168000	1.62	1.4	74.4
532k	532000	5.12	2.2	89.1
1866k	1866000	18.08	2.2	89.1

[a]The partial exclusion of the tracer from the brush can increase the effective diameter by up to ~80%.

either dPS(23k) or dPS(532k) at $\varphi_t = 0.10$. The best fits to the scattering intensity in Figure 3c were achieved using a core−shell model with one or four shells for the dPS(23k) and dPS(532k) systems, respectively (Supporting Information), where the shell thickness corresponds to the previously defined h_{eff}, which reflects the dPS penetration into the brush.[36] For dPS(23k) and dPS(532k) systems, the scattering length densities (SLD) that provide the best SANS fit (solid lines in Figure 3c) are plotted in Figure 3d,e. Because dPS(23k) can readily penetrate the PS(87k) brush, the SLD profile shows a gradual decrease in dPS volume fraction from 10 vol% in the matrix to 6.3 vol% for the single shell around the NP (Figure 3d). In contrast, for the dPS(532k) system, the SLD profile decreases more abruptly because of the limited penetration of dPS(532k) into the brush. To capture this behavior, four shells are used corresponding to 8.4, 4.1, 1.9, and 0 vol% dPS(532k). Note that the depletion of dPS(532k) extends to a distance of ~$2R_{g,b}$. The SLD profiles (Figure 3d,e) arising from the gradient of dPS within the brush are in excellent agreement with the SCFT calculations (Figure 3a,b), confirming that the penetration of the tracer molecules into the polymer brush is strongly determined by the tracer molecular weight relative to that of the brush. Therefore, large tracer molecules are unable to penetrate the brush, increasing the effective NP diameter by $2h_{eff}$. As noted in Table 1, d_{eff} can increase from 51 (core diameter) to 89 nm, for the highest tracer molecular weight systems.

For tracer diffusion in hard particle systems, the reduced diffusion coefficient (D/D_0), where D is normalized by the tracer diffusion coefficient in pure PS (D_0), was previously found to collapse on a master curve when plotted against the confinement parameter defined as the average interparticle distance relative to the probe size, namely, ID/$2R_g$.[23] This empirical parameter reflects the key length scales, namely, the space accessible to the diffusing chain (i.e., distance between impenetrable, immobile nanoparticles) relative to the size of that chain. Whereas prior studies were limited to hard particles and a narrow range of ID/$2R_g$, this study provides a much more stringent test of this simple scaling relationship by covering a much wider range of confinement parameter and exploring soft NPs that allow for tracer penetration and depletion from the brush. For both hard and soft NPs, Figure 4 shows that D/D_0 values collapse on a master curve when plotted as a function of ($ID_{eff}/2R_g$) over an extremely wide range of $ID_{eff}/2R_g$ for both hard and soft NPs. In addition, prior study showed similar scaling behavior of D/D_0 regardless of the size of nanoparticles, indicating universal scaling behavior of polymer diffusion.[24] Possible explanations for slowing down include: an increase in excluded volume, an increase in packing, the formation of an immobilized surface layer, an increase in entanglement density, and an increase in monomeric friction coefficient. No present

dx.doi.org/10.1021/mz400064w | ACS Macro Lett. 2013, 2, 485−490

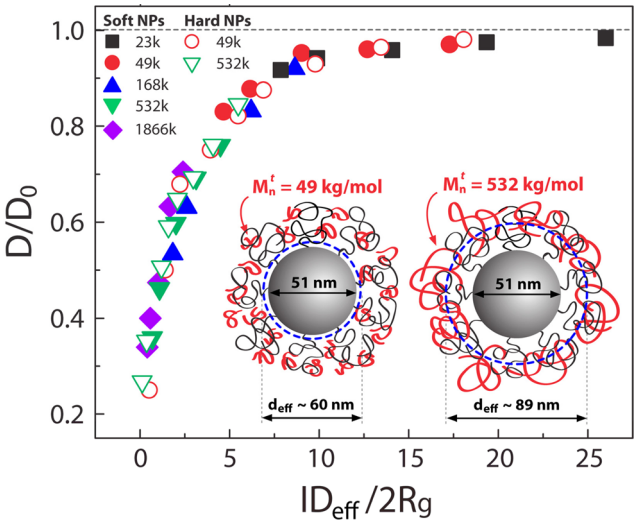

Figure 4. Effect of confinement parameter, defined as the interparticle distance relative to the tracer polymer size, on diffusion. The reduced diffusion coefficient (D/D_0) of dPS (M_n^t = 23, 49, 168, 532, and 1866 kg mol^{-1}) as a function of the confinement parameter $ID_{eff}/2R_g$ yields a master curve. Closed and open symbols represent dPS diffusion in nanocomposites with soft (SiO_2−PS87k) and hard (SiO_2−I) NPs, respectively. ID_{eff} was calculated using d_{eff} determined by SCFT calculations. Inset illustrates how penetration of the tracer into the polymer brush decreases as the tracer size increases which results in closer effective spacing of NPs (i.e., ID_{eff} decrease).

models can adequately explain the behavior of polymer diffusion shown in Figure 4.

In the presence of NPs, polymer diffusion slows down monotonically as $ID_{eff}/2R_g$ decreases. When NPs are very far apart relative to the tracer size (i.e., $ID_{eff}/2R_g \sim 10$), free or unconfined diffusion is observed. As confinement increases, initially, tracer diffusion slows down gradually, and then much more strongly when the average NP separation approaches the size of the tracer molecule (i.e., $ID_{eff}/2R_g < \sim 2$). For the first case, the bulk diffusion coefficient ($D/D_0 = 1$) is recovered at high values of $ID_{eff}/2R_g$ (i.e., >20). This is a previously unexplored regime because prior studies using hard spheres could only achieve a maximum value of ~3.[23,24] These results indicate that NPs separated by a distance 10 times the tracer size can slow diffusion. The origin of this long-range slowing down is presently unknown. These results are of great practical importance when formulating PNCs (i.e., selective particle size and concentration) such that they exhibit similar processing properties as the pure polymer. In the confined regime, diffusion is slowed down more strongly (~20%) than predicted by the simple Maxwell model, which accounts for only the impenetrable volume of the NP.[23] As will be proposed in our future paper, this slowing down in the confined regime may result from excluded volume that restricts the configurational entropy of the diffusing molecules through pore-like regions. Other potential explanations are given below. In this second regime, the reduced diffusion coefficients for both hard and soft NPs superpose, indicating that the polymer brush layers can increase the effective NP size and, correspondingly, reduce the effective distance between NPs. In the highly confined regime, $ID_{eff}/2R_g < \sim 2$, the reduced diffusion coefficient decreases more strongly than in the confined regime as $ID_{eff}/2R_g$ decreases. In this crowded environment, the tracer must either lose conformational entropy upon squeezing between NPs or continually probe its surrounding "cage" until a large opening is found. In either case, diffusion would be slowed down in this highly confined region. Upon replotting Figure 4 on a log−log plot, the data no longer collapse in the highly confined regime (see Supporting Information). Namely, when compared at the same $ID_{eff}/2R_g$ (<~2), diffusion in the soft NP system is faster than in the hard NP case. Thus, a more nuanced scaling relationship or model is needed to differentiate between diffusion through nanocomposites containing penetrable and impenetrable NPs in the highly confined regime.

When the confining dimensions are comparable to the tracer size ($ID_{eff}/2R_g < \sim 2$), the viscoelastic properties of entangled polymer melts can change. For example, a reduction in the entanglement density was attributed to lateral chain compression and the dilution of the interchain entanglement, leading to enhanced mobility in 1D and 2D confined polymer melts (e.g., large polymers in nanopores or ultrathin polymer films, respectively).[37,38] However, for bulk nanocomposites where polymers are three-dimensionally confined by nanofillers, NPs impose additional topological constraints on the diffusing polymer. Using neutron spin echo spectroscopy, Schneider et al. reported a significant reduction in apparent tube diameter for strongly confined polymer melts, where a transition in the tube constraints evolves from polymer entanglements to particle barriers as NP volume fraction increases.[19] Such tube constraints might contribute to the rapid decrease of the reduced diffusion coefficient with decreasing $ID_{eff}/2R_g$ in the highly confined regime ($ID_{eff}/2R_g < \sim 2$), as shown in Figure 4.

In conclusion, the diffusion of macromolecules in the presence of hard and soft NPs was investigated over a wide range of probe and matrix length scales. The reduced diffusion coefficient was found to collapse onto a master curve exhibiting a universal scaling behavior when plotted against a simple confinement parameter, $ID_{eff}/2R_g$. For soft NPs, the penetration of the tracer chains into the brush was independently modeled (SCFT simulations) and measured (SANS) to accurately define the interparticle spacing between NPs. Large tracer chains are partially excluded from the brush resulting in a reduced interparticle spacing relative to the hard NPs. Surprisingly, even a small volume fraction of NPs (0.05 vol%) corresponding to $ID_{eff}/2R_g \sim 10$ was found to slow down the diffusion of molecules. In the highly confined regime corresponding to high volume fractions of NPs (e.g., 50 vol%) and $ID_{eff}/2R_g < \sim 2$, the stronger decrease in diffusion may be attributed to an apparent decrease in tube diameter due to geometrical (NP) barriers that constrain the motion of polymers. Such a mechanism has been proposed but never observed experimentally for center of mass diffusion.[19] In addition to describing polymer dynamics, theoretical models of PNCs must account for the diffusion of NPs. For example, Yamamoto and Schweizer used PRISM theory to show that the faster than expected diffusion of NPs may be due to hydrodynamics.[39−41] In summary, $ID_{eff}/2R_g$ is a powerful guideline for understanding polymer dynamics in PNCs. Moreover, we have demonstrated the universal applicability of the confinement parameter by collapsing diffusion data from both hard and soft NP systems on a master curve, which provides a solid foundation on which to build theory.

dx.doi.org/10.1021/mz400064w | ACS Macro Lett. 2013, 2, 485−490

■ ASSOCIATED CONTENT

Supporting Information

The experimental details, self-consistent field theory, and analysis of SANS data. This material is available free of charge via the Internet at http://pubs.acs.org.

■ AUTHOR INFORMATION

Corresponding Author

*E-mail: composto@seas.upenn.edu.

Present Address

‡National Institute of Standards and Technology (NIST), Center for Neutron Research, 100 Bureau Drive, Gaithersburg, MD 20899, United States.

Notes

The authors declare no competing financial interest.

■ ACKNOWLEDGMENTS

This research was supported by the National Science Foundation NSF/EPSRC Materials World Network DMR-0908449 and DMR-1210379 (R.J.C., K.I.W.), EP/5065373/1 (N.C.) and Dupont CR&D (R.J.C.). Support was also provided by the NSF/MRSEC-DMR05-20020 (K.I.W., R.J.C.), and Polymer Programs DMR09-07493 (R.J.C.). M.J.A.H. acknowledges support from NSF/IGERT DGE02-21664. We also acknowledge the support of the National Institute of Standards and Technology, U.S. Department of Commence, in providing the neutron research facilities used in this work. This work utilized facilities supported in part by the National Science Foundation under Agreement No. DMR-0944772. The authors also thank H. Lee, C. M. Hui, and K. Matyjaszewski for discussions and comments on the particle synthesis.

■ REFERENCES

(1) Winey, K. I.; Vaia, R. A. *MRS Bull.* **2007**, *32*, 314−319.
(2) Collier, C. P.; Saykally, R. J.; Shiang, J. J.; Henrichs, S. E.; Heath, J. R. *Science* **1997**, *277*, 1978−1981.
(3) Lopes, W. A; Jaeger, H. M. *Nature* **2001**, *414*, 735−738.
(4) Taton, T. A.; Mirkin, C. A.; Letsinger, R. L. *Science* **2000**, *289*, 1757−1760.
(5) Vaia, R. A.; Maguire, J. F. *Chem. Mater.* **2007**, *19*, 2736−2751.
(6) Bockstaller, M. R.; Mickiewicz, R. A.; Thomas, E. L. *Adv. Mater.* **2005**, *17*, 1331−1349.
(7) Talley, C. E.; Jackson, J. B.; Oubre, C.; Grady, N. K.; hollars, C. W.; Lane, S. M.; Huser, T. R.; Nordlander, P.; Halas, N. J. *Nano Lett.* **2005**, *5*, 1569−1574.
(8) Balazs, A. C.; Emrick, T.; Russell, T. P. *Science* **2006**, *314*, 1107−1110.
(9) Zeng, H.; Li, J.; Liu, J. P.; Wang, Z. L.; Sun, S. *Nature* **2002**, *420*, 395−398.
(10) Shevchenko, E. V.; Talapin, D. V.; Kotov, N. A.; O'Brien, S.; Murray, C. B. *Nature* **2006**, *439*, 55−59.
(11) Tao, A.; Sinsermsuksakui, P.; Yang, P. *Nat. Nanotechnol.* **2007**, *2*, 435−440.
(12) Green, P. F. *Soft Matter* **2011**, *7*, 7914−7926.
(13) Kumar, S. K.; Jouault, N.; Benicewicz, B.; Neely, T. *Macromolecules* **2013**, *46*, 3199−3214.
(14) Meth, J. S.; Zane, S. G.; Chi, C.; Londono, J. D.; Wood, B. A.; Cotts, P.; Keating, M.; Guise, W.; Weigand, S. *Macromolecules* **2011**, *44*, 8301−8313.
(15) Hore, M. J. A.; Frischknecht, A. L.; Composto, R. J. *ACS Macro Lett.* **2012**, *1*, 115−121.
(16) Harton, S. E.; Kumar, S. K.; Yang, H.; Koga, T.; Hicks, K.; Lee, H.; Mijovic, J.; Liu, M.; Vallery, R. S.; Gidley, D. W. *Macromolecules* **2010**, *43*, 3415−3421.
(17) Hooper, J. B.; Schweizer, K. S. *Macromolecules* **2005**, *38*, 8858−8869.
(18) Bogoslovov, R. B.; Roland, C. M.; Ellis, A. R.; Randall, A. M.; Robertson, C. G. *Macromolecules* **2008**, *41*, 1289−1296.
(19) Schneider, G. J.; Nusser, K.; Wilner, L.; Falus, P.; Richter, D. *Macromolecules* **2011**, *44*, 5857−5860.
(20) Liu, J.; Cao, D.; Zhang, L.; Wang, W. *Macromolecules* **2009**, *42*, 2831−2842.
(21) Starr, F. W.; Schrøder, T. B.; Glotzer, S. C. *Macromolecules* **2002**, *35*, 4481−4492.
(22) Montes, H.; Lequeux, F.; Berriot, J. *Macromolecules* **2003**, *36*, 8107−8118.
(23) Gam, S.; Meth, J. S.; Zane, S. G.; Chi, C.; Wood, B. A.; Seitz, M. E.; Winey, K. I.; Clarke, N.; Composto, R. J. *Macromolecules* **2011**, *44*, 3494−3501.
(24) Gam, S.; Meth, J. S.; Zane, S. G.; Chi, C.; Wood, B. A.; Winey, K. I.; Clarke, N.; Composto, R. J. *Soft Matter* **2012**, *8*, 6512−6520.
(25) Composto, R. J.; Walters, R. M.; Genzer, J. *Mater. Sci. Eng., R* **2002**, *38*, 107−180.
(26) Matyjaszewski, K.; Miller, P. J.; Shukla, N.; Immaraporn, B.; Gelman, A.; Luokala, B. B.; Siclovan, T. M.; Kickelbick, G.; Vallant, T.; Hoffmann, H.; Pakula, T. *Macromolecules* **1999**, *32*, 8716−8724.
(27) Choi, J.; Dong, H.; Matyjaszewski, K.; Bockstaller, M. R. *J. Am. Chem. Soc.* **2010**, *132*, 12537−12539.
(28) Choi, J.; Hui, C. M.; Pietrasik, J.; Dong, H.; Matyjaszewski, K.; Bockstaller, M. R. *Soft Matter* **2012**, *8*, 4072−4082.
(29) Crank, J. *The Mathematics of Diffusion*, 2nd ed.; Clarendon Press: Oxford, 1975.
(30) Green, P. F.; Mills, P. J.; Kramer, E. J. *Polymer* **1986**, *27*, 1063−1066.
(31) Green, P. F.; Kramer, E. J. *Macromolecules* **1986**, *19*, 1108−1114.
(32) Wijmans, C. M.; Zhulina, E. B. *Macromolecules* **1993**, *26*, 7214−7224.
(33) Green, P. F. *Soft Matter* **2011**, *7*, 7914−7926.
(34) Voudourus, P.; Choi, J.; Gomopoulos, N.; Sainidou, R.; Dong, H.; Matyjaszewski, K.; Bockstaller, M. R.; Fytas, G. *ACS Nano* **2011**, *5*, 5746−5754.
(35) Hore, M. J. A.; Composto, R. J. *Macromolecules* **2012**, *45*, 6078−6086.
(36) Kinning, D. J.; Thomas, E. L. *Macromolecules* **1984**, *17*, 1712−1718.
(37) Si, L.; Massa, M. V.; Dalnoki-Veress, K.; Brown, H. R.; Jones, R. A. L. *Phys. Rev. Lett.* **2005**, *94*, 127801.
(38) Shin, K.; Obukhov, S.; Chen, J. T.; Huh, J.; Hwang, Y.; Mok, S.; Dobriyal, P.; Thiyagarajan, P.; Russell, T. P. *Nat. Mater.* **2007**, *6*, 961−965.
(39) Tuteja, A.; Mackay, M. E.; Narayanan, S.; Asokan, S.; Wong, M. S. *Nano Lett.* **2007**, *7*, 1276−1281.
(40) Grabowski, C. A.; Adhikary, B.; Mukhopadhyay, A. *Appl. Phys. Lett.* **2009**, *94*, 021903.
(41) Yamamoto, U.; Schweizer, K. S. *J. Chem. Phys.* **2011**, *135*, 224902.